Regular Article

ANALYTICAL
AND BIOANALYTICAL
CHEMISTRY
RESEARCH

Published by the
Iranian Chemical Society

***Anal. Bioanal. Chem. Res.**, Vol. 10, No. 1, 111-120, January 2023.*

Silica-Coated Magnetic Tragacanth Gum Nanoparticles Crosslinked with Citric Acid for the Loading and Delivery of Ranitidine

Fereshteh Farajian and Payman Hashemi*

Department of Chemistry, Faculty of Science, Lorestan University, Khoramabad, I.R. Iran

(Received 28 June 2022, Accepted 30 October 2022)

A new magnetic nanocomposite was prepared by synthesizing Fe_3O_4@SiO_2 nanoparticles and then coating them with a shell of tragacanth gum (TG) as a natural product modified by citric acid (CA). The prepared Fe_3O_4@SiO_2@TG-CA nanoparticles were identified by scanning electron microscopy (SEM), energy dispersive X-ray analysis (EDX), and Fourier transform infrared spectroscopy (FT-IR). The prepared magnetic nanoparticles were used for loading and delivery of ranitidine, an oral drug. Conditions for drug loading were optimized by a central composite design optimization method. The maximum loading efficiency for ranitidine was 79.3%, obtained at pH 11 and, its *in vitro* release was gained within 55 min at pH 1.6 in a phosphate buffer medium. The loading capacity of the nanocarrier was dependent on the initial concentration of ranitidine and exceeded 11.4 mg g^{-1} for a 200 mg l^{-1} solution. The study of adsorption isotherms to describe the interaction of ranitidine with the carrier showed the best fit with Freundlich isotherm. The results showed that the prepared Fe_3O_4@SiO_2@TG-CA adsorbent, as a non-toxic and low-cost nanocarrier, is quite suitable for drug delivery applications.

Keywords: Magnetic nanoparticles, Tragacanth gum, Citric acid, Drug delivery, Hydrogel

INTRODUCTION

Hydrogels are hydrophilic three-dimensional polymers containing a crosslinked network of hydrophilic water-soluble polymers. They absorb huge amounts of water and tend to swell [1]. They are appropriate for the encapsulation and delivery of drugs due to their unique physical properties. Both synthetic and natural hydrogels have been applied to drug delivery tasks [2]. However, natural hydrogels are more suitable due to their intrinsic biocompatibility and biodegradability [3]. Xanthan gum, gellan gum, cellulose, starch, chitosan, and tragacanth gum (TG) are some well-known natural polymers used to make hydrogels for drug delivery applications [4].

TG is a natural viscous mixture of polysaccharides obtained from the root of its plant. It is a biosorbent hydrogel bead that is non-toxic, abundant, low-cost, and biocompatible [2,3]. TG can be modified by various functional groups such as carboxylic acid, primary and secondary hydroxyl, and epoxy groups. This will increase its selectivity and provides favorable adsorption conditions. TG has been used in many applications such as wound dressing [5], drug delivery [6], natural preservative [7,8], and suspending and thickening agent [9]. TG is a biodegradable, biocompatible, odorless, tasteless, osteogenic, and stable biopolymer over a wide pH range [10,11]. However, pure TG alone has some weaknesses, and therefore, it is often reinforced with either organic or inorganic fillers such as clays [12], carbon nanotubes [13], and metal oxides [14]. In addition, incorporating magnetic nanoparticles (NPs) in polymeric beads can facilitate their separation from the solution and increase the loading capacity of the bead due to enhanced electrostatic interactions [15]. It also enables control of the drug release profiles [16].

Natural hydrogels or biopolymers can be crosslinked either physically or chemically. Physically crosslinked

*Corresponding author. E-mail: hashemi.payman@gmail.com

natural hydrogels are not so robust and, their network structure may change by varying pH, ionic strength, or temperatures of the environment [11]. Although chemically crosslinked hydrogels are more stable, the crosslinking molecules used to make them may be toxic [6]. Citric acid has appeared as a non-toxic cross-linking agent in recent years for the manufacture of hydrogels [13]. High temperatures, causes citric acid to esterify the -OH groups of an adjacent polymer chain by making a cyclic anhydride and forming crosslinks [17].

The present study aims to describe a novel synthesis of a Fe_3O_4@SiO_2@TG nanocomposite crosslinked with citric acid as a magnetic nanocarrier with biocompatibility, low toxicity, and low cost. The SiO_2 shell is expected to increase the stability of the NPs in acidic conditions. The synthesized nanocomposite is applied to the loading and delivery of ranitidine as a model compound. Ranitidine is a histamine H_2-receptor antagonist medicine that has been used in the treatment of gastroduodenal ulcers and related diseases [18]. Multivariate methods are used for the optimization of the loading conditions in addition to the study of the adsorption mechanisms.

EXPERIMENTAL

Chemicals and Apparatus

Iron(III) chloride ($FeCl_3.6H_2O$), iron(II) chloride ($FeCl_2.4H_2O$), ammonia solution 25%, sodium hydroxide, tetraethyl orthosilicate (TEOS), and ethanol (EtOH) were purchased from Merck company and used without purification. Ranitidine hydrochloride was received from Exir Pharmaceuticals Ltd, Boroujerd, Iran. A stock solution (1000 mg g^{-1}) of ranitidine was made up by dissolving the required amount of its powder in pure water. Phosphate-buffered saline solution with a concentration of 0.15 M was used to adjust the pH of thee test samples. TG was obtained from residential natural resources. All solutions were prepared with deionized water. Sodium hypophosphite (SHP) as catalyst (Sigma-Aldrich, Germany), glycerol as a plasticizer, and citric acid (CA) as crosslinker (Merck, Germany) were used. All the spectrophotometric measurements of ranitidine were performed at its λ_{max} (232 nm) by a Shimadzu UV-1650PC UV-Vis. model Q124) was used for absorbance measurements.

Fourier transform infrared (FT-IR) spectra were recorded by KBr pellet technique on a Shimadzu, model 8400 (Japan), spectrometer. A field emission scanning electron microscope (FE-SEM) model Tescan Mira3 LMU (Czech Republic), equipped with an energy dispersive x-ray spectrometer (EDX), was used for the study of the adsorbent morphology and analysis. The X-ray diffraction (XRD) patterns of samples were obtained with a Philips PANalytical X'Pert XRD system using Cu-Kα radiation of wavelength 0.154 nm.

For the measurement of hydrodynamic sizes and zeta potential values of the NPs, an SZ-100-HORIBA (Japan) dynamic light scattering (DLS) analyzer was used. The particles were diluted with 20% ethanol in deionized water (pH 7).

Synthesis of Fe_3O_4 NPs

Fe_3O_4 NPs were synthesized by a standard chemical co-precipitation method [19]. Briefly, 50 ml of 0.001 M equimolar solution of $FeCl_3.6H_2O$, and $FeCl_2.4H_2O$ was prepared in deionized water. The mixture of the iron salts was sonicated for 15 min at room temperature. It was then transferred to a round bottom two-neck flask and heated to 80 °C under reflux in an argon atmosphere. Then, 5 ml ammonia (25 wt%) was slowly added to the mixture for 30 min. A color change from yellowish to black was observed and the blend was further heated to 90 °C for 1.5 h. Then, the obtained Fe_3O_4 NPs were collected and separated using a permanent magnet, washed vigorously with pure water, and re-suspended in 100 ml of deionized water. The obtained NPs were stable in this condition for up to one month.

Synthesis of Fe_3O_4@SiO_2 NPs

For the silanization of the magnetic NPs, a typical Stöber method was used. For this purpose, 1.5 g of Fe_3O_4 NPs were dispersed in a mixture of 16 ml distilled water, 2 ml 25% ammonia, and, 80 ml ethanol and sonicated for 15 min in an ultrasonic bath. After that, 1.0 ml of tetraethyl orthosilicate (TEOS) was added dropwise to the solution containing the NPs. The suspension was shaken in a shaker bath for 24 h at room temperature. Lastly, the NPs were separated by the magnet and vigorously washed with pure water.

Coating of Fe_3O_4@SiO_2 NPs with TG and Citric Acid

A 2% solution of TG was prepared by dissolving 0.02 g

of TG powder in 10 ml of hot water (80 °C). To the silica-coated NPs, 10 ml of a 2% solution of TG was added and stirred at room temperature for 8 h. TG is expected to couple to the Fe_3O_4@SiO_2 NPs by the formation of hydrogen bonds. The black product was separated by a permanent magnet.

The TG coating of the NPs was then crosslinked by citric acid as a biocompatible crosslinker according to the method reported by Awadhiya *et al*. with some modifications [20]. For this purpose, a 20 ml solution containing 2.0 g citric acid, 0.04 g TG, 1.0 g sodium hypophosphite as a catalyst, and 0.2 g glycerol as a plasticizer was added to the NPs. The mixture was heated to 80 °C and mixed for 24 h under magnetic stirring. The prepared NPs were then washed and rinsed three times with deionized water. The resulting NPs were black and, due to high water absorption, their size increased several times, indicating that they were covered with TG. Magnetic particles coated with TG and citric acid (Fe_3O_4@SiO_2@TG-CA) were kept in water at 4 °C. A schematic of the preparation of the magnetic NPs with the coating of TG is shown in Fig. 1.

Central Composite Design (CCD) Optimization

The effects of four factors on the adsorption loading efficiency of ranitidine were optimized using a CCD optimization method. The loading efficiency was calculated according to the following equation:

$$\text{Loading efficiency (\%)} = \frac{(C_0 - C_e)}{C_0} \times 100$$

in which C_0 and C_e are the drug concentrations (mg l^{-1}) at initial and equilibrium time, respectively.

Sample volume, adsorbent weight, contact time, and, pH

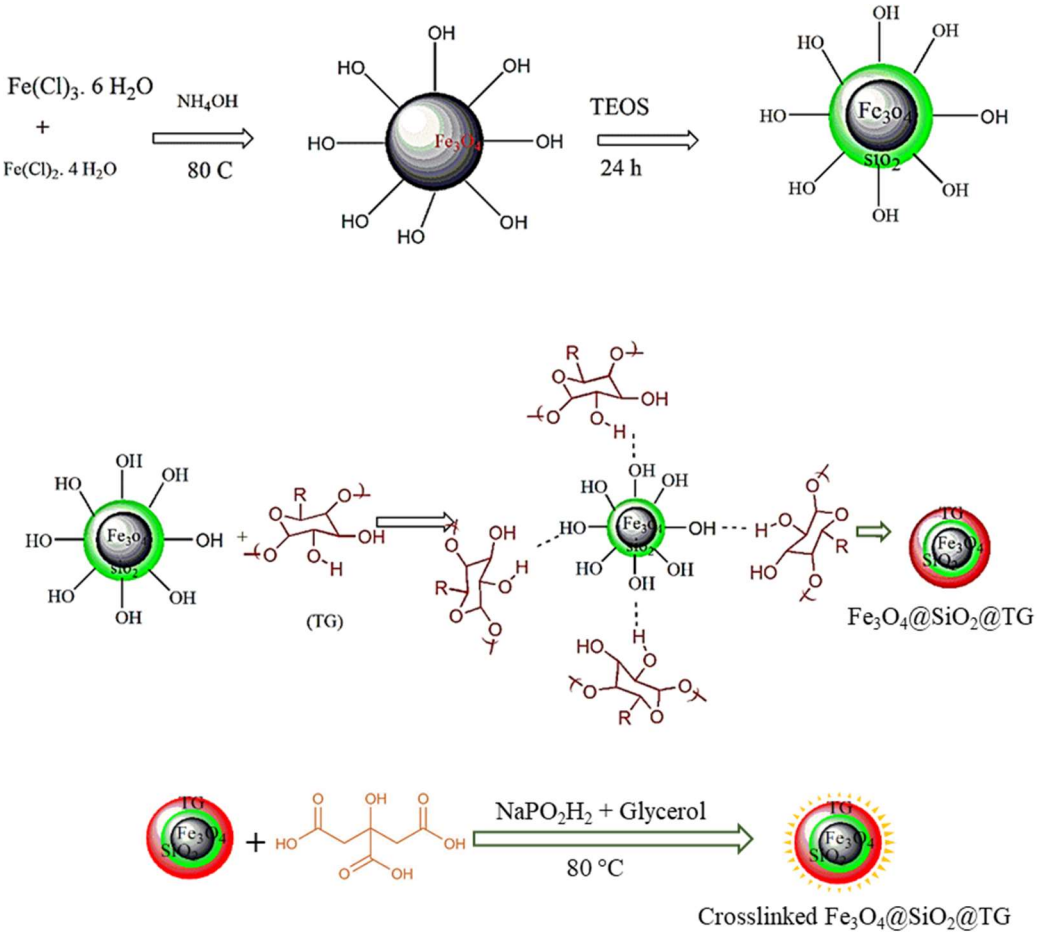

Fig. 1. A schematic representation of the synthesis of the Fe_3O_4@SiO_2@TG nanoparticles.

Table 1. The Studied Factors and Levels for the CCD Optimization

Factor	Abbreviation	Factors' levels				
		-α	Low	0	High	+α
pH	pH	2	3.5	5	6.5	8
Contact time (min)	Time	20	30	40	50	60
Temperature (°C)	T	25	30	35	40	45
Sample volume (ml)	V_s	1	3	5	7	9

of the test solutions were the four factors studied by CCD. Low and high levels for each factor were taken based on the results of some initial trials. The four factors examined using the CCD model and the five levels developed for each parameter are shown in Table 1. For optimization, the software package of Minitab 16 was used and the recovery of the drug was regarded as the response function.

A drug concentration of 20 mg l^{-1} with the pH adjusted by phosphate-buffered saline solution (0.15 M) was used during the optimization. Fe_3O_4@SiO_2@TG-CA NPs were added and, the solution was mixed at room temperature on a shaker bath for a fixed time. Then, the nanocomposite was collected by a permanent magnet. The amount of loaded ranitidine was evaluated by the absorbance measurements at 232 nm before and after the adsorption. Standard solutions of ranitidine were used for the calibration.

Calculation of the Loading Capacity

For the evaluation of the loading capacity of the magnetic NPs in mg g^{-1}, their loading in different drug concentrations was determined. The nanocarrier NPs (5 mg) were added to 1 ml of a drug solution at pH 11. The residual amount of the drug in the supernatant was measured by the UV-Vis spectrophotometer (at 232 nm).

Study of the Drug Release

For evaluation of the in vitro release of ranitidine drug from the nanocarrier, 40 mg of the loaded NPs were suspended in 5 ml of phosphate-buffered saline in various pHs. The NPs were already loaded with 1 ml of a 20 mg l^{-1} solution of ranitidine in pH 11 for 50 min. For calculation of the released percent of the drug, the mg released drug in the solution times 100 was divided by the mg loaded medicine on the adsorbent.

RESULTS AND DISCUSSION

Characterization of the NPs

In the preliminary experiments, Fe_3O_4, Fe_3O_4@SiO_2, and Fe_3O_4@SiO_2@TG magnetic NPs were prepared and characterized by FT-IR, SEM, EDX, XRD, and, DLS analyses. Figure 2 shows the FT-IR spectra of the NPs. In the FT-IR spectrum of Fe_3O_4 NPs (Fig. 2a), the band that appeared at 567 cm^{-1} is related to stretching vibrations of Fe-O. The wide adsorption band, around 3400 cm^{-1} can be ascribed to stretching and bending vibrations of OH. The broad high-intensity absorption band at 1092 cm^{-1} in Fig. 2b is related to the asymmetric stretching of Si-O-Si in SiO_2. The absorption band at 802 cm^{-1} is assigned to the Si-O-Si symmetric stretch, and the absorption band at 466 cm^{-1} corresponds to the Si-O-Si or O-Si-O bending modes. The band at 458 cm^{-1} is ascribed to the Si-O-Si or O-Si-O bending

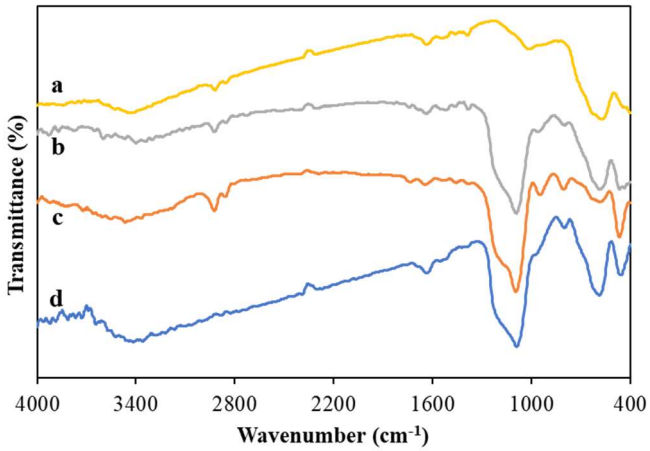

Fig. 2. FT-IR spectra of Fe_3O_4 (a), Fe_3O_4@SiO_2 (b), Fe_3O_4@SiO_2@TG-CA (c) and, ranitidine loaded Fe_3O_4@SiO_2@TG-CA (d).

modes. The absorption band at 2920 cm^{-1} in Fig. 2c is related to stretching vibrations of C–H. This band is an indication of the fixation of the TG layer on $Fe_3O_4@SiO_2$ magnetic NPs. For citric acid, a band at 1720 cm^{-1} is observed due to hydrogen bond C=O stretching and a broad band around 3400 cm^{-1} that corresponds to -OH stretching. In Fig. 2d, a band at 1627 has appeared that is assigned to the C=C-NO_2 stretching of ranitidine. The small band at 1377 cm^{-1} also can be attributed to the stretching band of the N-O group.

The size and morphology of $Fe_3O_4@SiO_2@TG$, $Fe_3O_4@SiO_2$, and, Fe_3O_4, NPs were studied by SEM. Figure 3 indicates the spherical morphology and narrow size distribution of the NPs with an average size of 50-70 nm for $Fe_3O_4@SiO_2@TG$. Energy dispersive X-ray (EDX) analysis was applied for the elemental mappings and distribution study of the prepared $Fe_3O_4@SiO_2$ and $Fe_3O_4@SiO_2@TG$ nanocomposites. Elements C, N, O, Si, and, Fe were detected based on EDX analysis (Table 2). Observation of some low C and N contaminations in $Fe_3O_4@SiO_2$ and other samples is not uncommon [21]. However, as predictable, the carbon content of $Fe_3O_4@SiO_2@TG$-CA NPs was more than that of $Fe_3O_4@SiO_2@TG$ and $Fe_3O_4@SiO_2$. In addition, decreasing the percentages of Si and Fe after coating the $Fe_3O_4@SiO_2$ nanocomposite by TG and CA, confirm the core-shell structure of the NPs. In general, FT-IR, SEM, and, EDX analyses established the formation and expected structures of the magnetic $Fe_3O_4@SiO_2$ and their coverage by TG and CA.

Zeta potential study of synthesized NPs resulted in potentials of -26.6, -23.0 and, -21.3 mV for the $Fe_3O_4@SiO_2$, $Fe_3O_4@SiO_2@GT$ and, $Fe_3O_4@SiO_2@GT@CA$ nanocarriers, respectively. Therefore, covering the NPs by TG and their crosslinking by CA moderately reduces their negative charges. The DLS results showed narrow size distribution of the particles and an increase of their sizes in

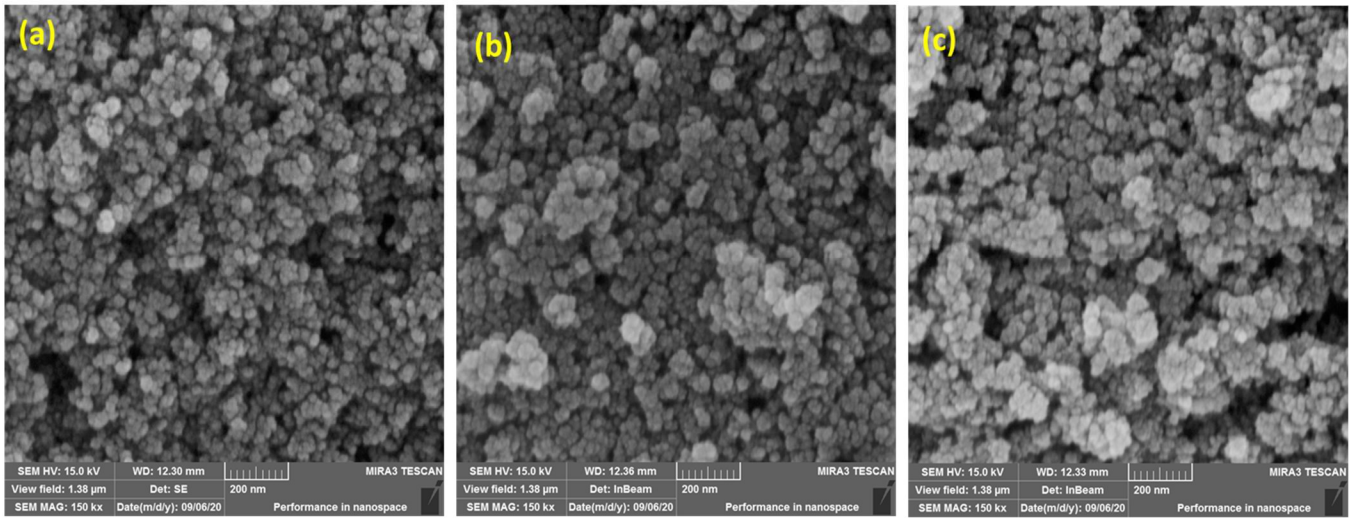

Fig. 3. SEM images of Fe_3O_4 (a), $Fe_3O_4@SiO_2$ (b) and, $Fe_3O_4@SiO_2@TG$-CA (c) NPs.

Table 2. The Percentages of the Elements Obtained by EDX Analysis in the $Fe_3O_4@SiO_2$, $Fe_3O_4@SiO_2@TG$ and $Fe_3O_4@SiO_2@TG$-CA

	Element compositions (%)				
Sample type	C	N	O	Si	Fe
$Fe_3O_4@SiO_2$	10.1	6.0	59.4	9.3	15.2
$Fe_3O_4@SiO_2@TG$	33.82	6.95	54.34	1.16	3.73
$Fe_3O_4@SiO_2@TG$-CA	57.08	6.01	34.81	0.63	1.47

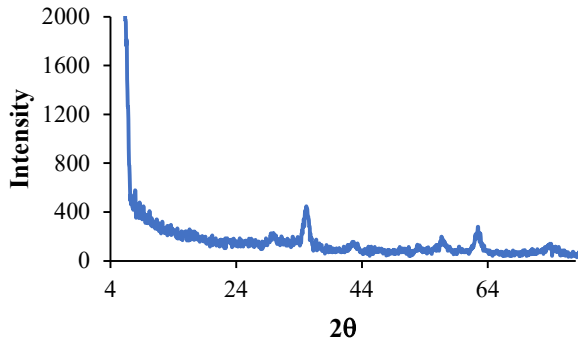

Fig. 4. The XRD spectrum of the Fe3O4@SiO2@GT@CA nanocarrier.

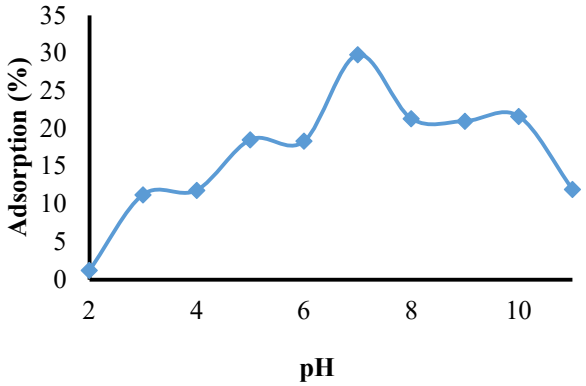

Fig. 5. Effect of pH on the loading of ranitidine on the Fe_3O_4@SiO_2@TG-CA NPs. Sample volume, 5 ml; adsorbent mass, 50 mg; drug concentration, 20 mg l^{-1}; mixing time, 30 min; temperature, 25 °C.

aqueous solution to 181.5, 223.6, and 260.2 nm, respectively. This indicates the biocompatible hydrogel coating of the nanocarriers for the incorporation of the drug [22].

Figure 4 indicates the XRD spectrum of the Fe_3O_4@SiO_2@GT@CA prepared adsorbent. The figure exhibits a sharp diffraction peak at 2θ of 4.44° and other typical diffraction peaks at 2θ of 29.8, 35.2, 42.6, 56.7, 62.4, and, 73.9°. The XRD pattern of the Fe_3O_4@SiO_2@GT@CA NPs agreed with the reported patterns in the literature [23].

Effect of pH on Loading

One of the basic parameters in loading systems is pH, which influences both the chemistry of the sample and the adsorbent binding sites [24]. In the present study, the effect of pH on the adsorption or loading of the drug was investigated in the range of pH = 2-11. The initial drug concentration in this study was 20 mg l^{-1} using 50 mg of the NPs and a mixing time of 30 min (Fig. 5). Variation in pH can change the surface charge of magnetic NPs [25]. More negative surface charges are expected in a higher pH that is more appropriate for the extraction of ranitidine with more or less positively charged groups. This criterion is established by the increase in the efficiency of adsorption between pH 2 to 7 in Fig. 5. However, in a pH higher than 7, the positive charges on the drug are decreased. As a result, lower loadings are observed.

Optimization by Central Composite Design (CCD)

CCD is one of the suitable multivariate optimization techniques. In this procedure, a factorial test plan is combined with an additional axis or Starpoint and at least one midpoint. This model can estimate both linear and quadratic effects [26]. The midpoint is usually repeated to correctly assess the experimental error [27].

For CCD optimization of the experimental parameters in this work, four factors of pH, sample volume (Vs), temperature (T), and, mixing time were studied. The levels of the variables in 31 designed experiments by the model and the obtained response values for each experiment have been presented in Table 3. Simultaneous optimization of the studied factors was performed using a response surface model. Some three-dimensional response plots have been shown in Fig. 6 to indicate how the response variable changes with changing a pair of variables, keeping the others constant.

As revealed in Fig. 6a, in a high pH, a decrease in loading is observed which is increased over time. In a lower pH, the mixing time does not significantly influence the loading efficiency of ranitidine, stating a faster adsorption process. Figure 6b indicates a decrease in adsorption by increasing the time in all the studied temperatures, with little interaction. In Fig. 6c, it is shown that in a high temperature, loading is decreased by time, but in a low temperature, an opposite effect is encountered.

Table 4 shows the results of the data analysis by the CCD model for the individual and squared effects and second-order interactions of the studied variables. According to the t-test results, the most significant variable is the sample

Table 3. The Conditions of the Planned Experiment and the Respective Response Values Obtained by Performing the CCD Optimization Experiment

Run order	pH	V_s (ml)	Time (min)	T (°C)	Loading (%)
1	7	5	30	30	32.9
2	8	7	20	35	33.5
3	10	7	20	35	23.8
4	8	3	20	35	55.9
5	10	3	20	25	51.7
6	8	3	40	25	51.0
7	9	5	30	30	30.1
8	10	7	40	35	21.8
9	8	7	40	35	34.9
10	9	5	50	30	27.3
11	9	9	30	30	21.0
12	10	7	20	25	23.8
13	8	3	20	25	53.1
14	9	5	30	30	33.5
15	9	5	30	20	29.1
16	8	7	20	25	36.0
17	10	7	40	25	29.6
18	11	5	30	30	26.4
19	8	7	40	25	31.3
20	8	3	40	35	23.8
21	9	1	30	30	76.3
22	9	5	30	30	29.6
23	9	5	10	30	28.1
24	10	3	40	25	50.8
25	9	5	30	30	33.7
26	9	5	30	30	42.6
27	10	3	40	35	55.2
28	9	5	30	40	30.0
29	10	3	20	35	51.6
30	9	5	30	30	33.6
31	9	5	30	30	29.8

volume, with a large negative impact on the loading efficiency. The other factors are statistically insignificant

Table 4. Effects of the Factors, Coded Coefficients (Coef), Standard Errors (SE) of the Coefficients, t-Values and p-Values of the Variables Obtained by the CCD Model

Term.	Effect	Coef.	SE Coef	t-Value	p-Value
Constant		33.30	2.57	12.98	0.000
pH	-1.96	-0.98	1.39	-0.71	0.490
Time	-2.77	-1.39	1.39	-1.00	0.332
T	-2.14	-1.07	1.39	-0.77	0.451
Vs	- 22.47	- 11.24	1.39	-8.11	0.000
pH×pH	-0.06	-0.03	1.27	-0.02	0.983
Time×Time	-1.03	-0.52	1.27	-0.41	0.690
T×T	-0.11	-0.05	1.27	-0.04	0.967
Vs×Vs	9.44	4.72	1.27	3.72	0.002
pH×Time	5.59	2.79	1.70	1.65	0.119
pH×T	2.56	1.28	1.70	0.75	0.461
pH×Vs	-7.69	-3.84	1.70	-2.26	0.038
Time×T	-3.49	-1.74	1.70	-1.03	0.320
Time×Vs	3.91	1.96	1.70	1.15	0.266
T×Vs	1.59	0.79	1.70	0.47	0.646

with the order of Time > T > pH. The squared term of Vs^2 and the pH × V_s interaction were also significant, but the other squared terms and interactions were insignificant.

The predictive optimization conditions evaluated by the model were pH = 11, sample volume = 1.0 ml, temperature = 20 °C, and contact time = 50 min. Under the optimization conditions proposed in the model, the loading efficiency of ranitidine was 79.3% for six replicates with a relative standard deviation of 4.06%.

Loading Capacity

The loading capacity of the Fe_3O_4@SiO_2@TG-CA nanocarrier or its maximum ranitidine loading was dependent on the initial concentration of the drug in the sample. The capacity was calculated by suspending different amounts of the adsorbent in a buffered solution of the analyte, under the optimized conditions. The effect of the initial concentration of ranitidine on the loading capacity is shown in Fig. 7. The

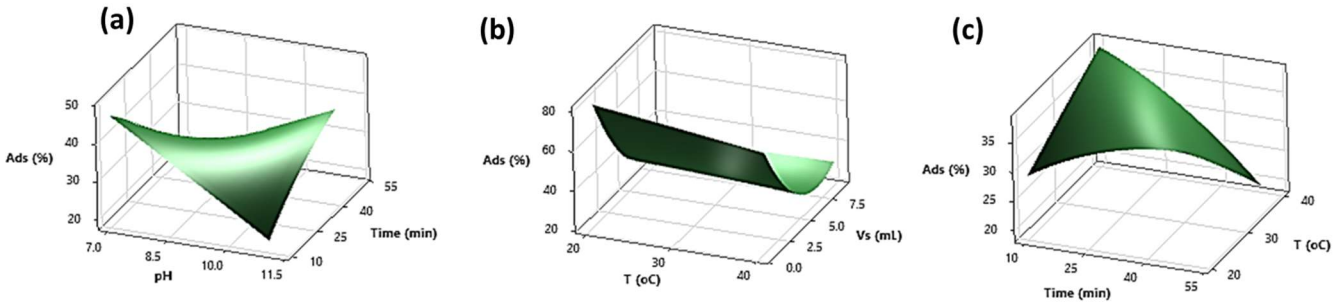

Fig. 6. Three-dimensional surface plots of the studied factors in CCD optimization. (a) Effects of pH and time, (b) Effects of temperature (T) and sample volume (V_s), (c) Effects of time and temperature (T) on the adsorption (Ads) of ranitidine.

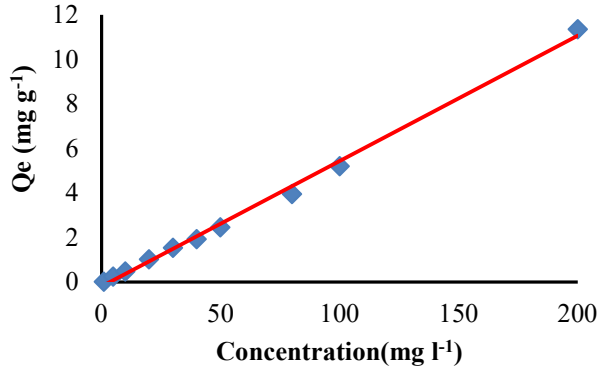

Fig. 7. Effect of the initial concentration of ranitidine on the loading capacity of NPs under the optimized conditions; pH, 7; T, 25 °C, t, 20 min, sample volume, 1.0 mL; adsorbent mass, 40 mg.

loading capacity of the nanocomposite increased by increasing the ranitidine concentration. The maximum capacity was obtained for 200 mg l^{-1} of ranitidine to be 11.4 mg g^{-1}. Higher ranitidine concentrations were not used due to the risk of its precipitation.

Study of the Adsorption Isotherms

The mechanism of interaction of ranitidine with the adsorbent was investigated by studying the adsorption isotherms in batch experiments. Freundlich and Langmuir's adsorption models were applied to investigate the adsorption mechanism. The Langmuir isotherm corresponds to the monolayer adsorption of a species onto the nanocomposite surface containing a fixed number of well-defined sites. According to this model, the plot of C_e/q_e, in which C_e is the equilibrium concentration of the analyte in solution and q_e is the equilibrium adsorption capacity of the sorbent, *versus* C_e, should be linear. The Freundlich isotherm works for reversible adsorption and is not restricted to establishing a monolayer. According to this model, a linear plot is obtained for plotting $\log q_e$ *vs.* $\log C_e$ [21].

Figures 8a and 8b are the corresponding plots of the Langmuir and Freundlich models, respectively. Regarding R^2 as a parameter that indicates the desirability of fitting experimental results, the Freundlich model with an R^2 value of 0.9635 is more suitable than the Langmuir model, which suggests the potential for a multi-layer adsorption process for NPs. The k_F and n (Freundlich constants) were calculated to be 0.262 and 0.992, respectively. The k_F (mg g^{-1}) is a measure of the relative loading capacity of the nanocarrier, and n is an estimation of the intensity of the sorption. A value of 1/n less than or greater than one indicates a normal Langmuir isotherm or cooperative sorption, respectively [28].

Evaluation of the Drug Release

The effect of contact time on the desorption or the release rate of ranitidine from the sorbent was investigated in the range of 1-55 min. Ranitidine was first loaded on the nanocarrier in the optimized conditions (pH = 11, the volume of sample = 1.0 ml, T = 20 °C and contact time = 50 min). The release was carried out using phosphate-buffered saline in pHs of 1.6, 3.0, 5.5, and, 7.4 (Fig. 9). The best result was obtained in pH 1.6, which is the pH with minimum loading of the drug (see Fig. 5). The maximum drug release was 80.4 (±2.7)% that was achieved within 55 min in pH 1.6.

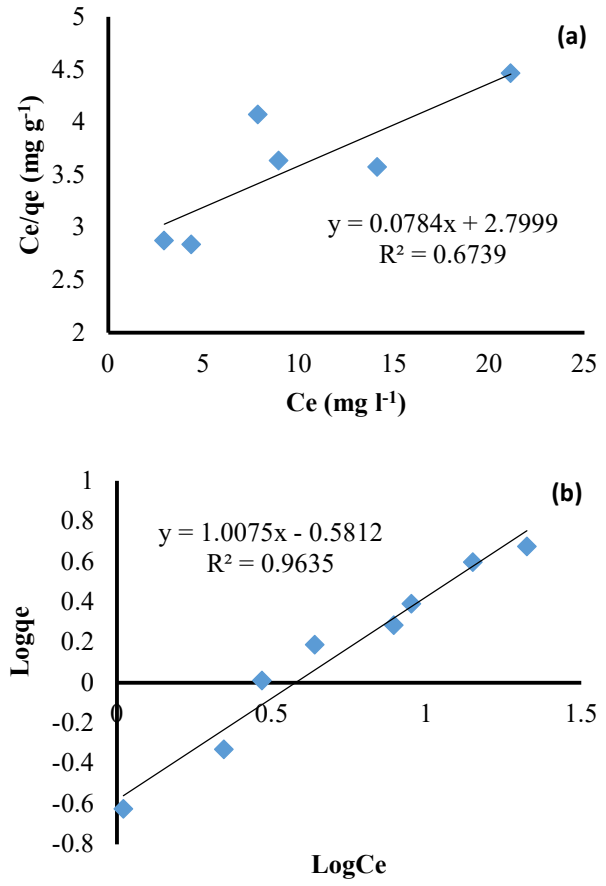

Fig. 8. Langmuir (a) and Freundlich (b) adsorption isotherms for the data of Fig. 7.

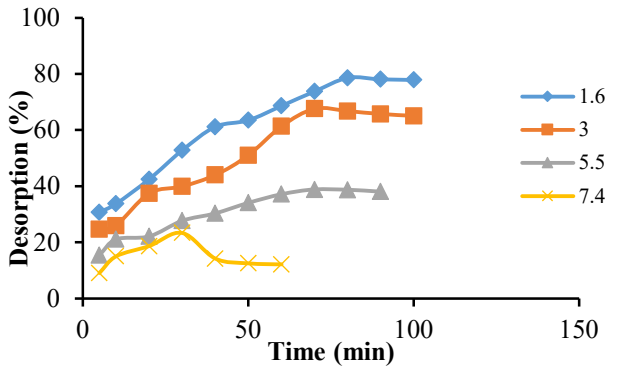

Fig. 9. Ranitidine release (delivery) from the loaded Fe_3O_4@SiO_2@TG-CA NPs in pHs of 1.6, 3.0, 5.5 and, 7.4.

CONCLUSIONS

Coating of Fe_3O_4@SiO_2 magnetic NPs by TG as a natural hydrogel was successfully performed using a simple modifying process. Characterization of the prepared NPs by FT-IR, EDX, and, SEM confirmed the structure and the relatively uniform sizes of the prepared NPs. The results indicated that the synthesized Fe_3O_4@SiO_2@TG-CA nanocomposite is an appropriate carrier for the loading and releasing of ranitidine, as it is non-toxic, highly porous, low cost, and, biocompatible.

The modified nanocomposite indicated a high efficiency for ranitidine adsorption with a loading capacity of up to 11.4 mg g^{-1}, in a short time. The adsorption on the prepared NPs was best fitted into the Freundlich isotherm. Delivery of the medicine at pH 1.6 within 50 min, suggests a slow release of the drug in the stomach. It may be concluded from the results that Fe_3O_4@SiO_2@TG-CA, as an inorganic-organic hybrid, can be potentially applied for the loading and delivery of ranitidine and probably for the removal of pharmaceutical residues in the environment.

REFERENCES

[1] A.H. Shalla, M.A. Bhat, Z. Yaseen, J. Environ. Chem. Eng. 6 (2018) 5938.
[2] S. Nasirimoghaddam, S. Zeinali, S. Sabbaghi, J. Ind. Eng. Chem. 27 (2015) 79.
[3] S. Sadeghi, F.A. Rad, A.Z. Moghaddam, Mater. Sci. Eng. C. 45 (2014) 136.
[4] T.R. Bhardwaj, M. Kanwar, R. Lal, A. Gupta, Drug Dev. Ind. Pharm. 26 (2000) 1025.
[5] R. Sahraei, Z.S. Pour, M. Ghaemy, J. Clean. Prod. 142 (2017) 2973.
[6] B. Singh, L. Varshney, S. Francis, Radiat. Phys. Chem. 135 (2017) 94.
[7] B. Singh, V. Sharma, Carbohydr. Polym. 157 (2017) 185.
[8] M. Nasiri, M. Barzegar, M.A. Sahari, M. Niakousari, Food Hydrocoll. 72 (2017) 202.
[9] A. Komeilyfard, M. Fazel, H. Akhavan, A. Mousakhani Ganjeh, J. Texture Stud. 48 (2017) 114.
[10] R. Sahraei, M. Ghaemy, Carbohydr. Polym. 157 (2017) 823.

[11] S. Kulanthaivel, S.R. VS, T. Agarwal, S. Pradhan, K. Pal, S. Giri, T.K. Maiti, I. Banerjee, J. Mater. Chem. B 5 (2017) 4177.

[12] S. Mallakpour, S. Rashidimoghadam, Recent Developments in the Synthesis of Hybrid Polymer/clay Nanocomposites: Properties and Applications, in: Hybrid Polymer Composite Materials, Elsevier, 2017, pp. 227.

[13] S. Mallakpour, V. Behranvand, Recent Progress and Perspectives on Biofunctionalized CNT hybrid Polymer Nanocomposites, in: Hybrid Polymer Composite Materials, Elsevier, 2017, pp. 311.

[14] S. Mallakpour, S. Rashidimoghadam, Investigation on morphology, properties, and applications of hybrid poly (vinyl chloride)/metal oxide composites, in: Hybrid Polymer Composite Materials, Elsevier, 2017, pp. 343.

[15] Y. Zhou, S. Fu, L. Zhang, H. Zhan, M.V. Levit, Carbohydr. Polym. 101 (2014) 75.

[16] K. Hemmati, A. Masoumi, M. Ghaemy, Carbohydr. Polym. 136 (2016) 630.

[17] K. Mali, S. Dhawale, R. Dias, N. Dhane, V. Ghorpade, Indian J. Pharm. Sci. 80 (2018) 657.

[18] R. Pahwa, S. Sharma, V. Kumar, K. Kohli, J. Chem. Pharm. Res. 8 (2016) 70.

[19] M. Faraji, Y. Yamini, E. Tahmasebi, A. Saleh, F. Nourmohammadian, J. Iran. Chem. Soc. 7 (2010) S130.

[20] A. Awadhiya, D. Kumar, V. Verma, Carbohydr. Polym. 151 (2016) 60.

[21] F. Ghanbari Adivi, P. Hashemi, A. Dadkhah Tehrani, Polym. Bull. 76 (2019) 1239.

[22] J. Szűcsová, A. Zeleňáková, O. Kapusta, A. Berkutova, V. Zeleňák, in: AIP Conference Proceedings, AIP Publishing LLC, 2018, pp. 020047.

[23] J. Xu, C. Ju, J. Sheng, F. Wang, Q. Zhang, G. Sun, M. Sun, Bull. Korean Chem. Soc. 34 (2013) 2408.

[24] Z.L. Yaneva, N.V. Georgieva, IRECHE 4 (2012) 127.

[25] K. Ahalya, N. Suriyanarayanan, S. Sangeetha, Mater. Sci. Semicond. Process. 27 (2014) 672.

[26] M.A. Bezerra, R.E. Santelli, E.P. Oliveira, L.S. Villar, L.A. Escaleira, Talanta 76 (2008) 965.

[27] F.N. Serenjeh, P. Hashemi, M. Safdarian, Z. Kheirollahi, J. Iran. Chem. Soc. 11 (2014) 733.

[28] G. Limousin, J.-P. Gaudet, L. Charlet, S. Szenknect, V. Barthes, M. Krimissa, Appl. Geochem. 22 (2007) 249.